ACS APPLIED MATERIALS & INTERFACES

Research Article

www.acsami.org

Graphene Size Control via a Mechanochemical Method and Electroresponsive Properties

Keun-Young Shin, Seungae Lee, Seunghee Hong, and Jyongsik Jang*

World Class University (WCU) Program of Chemical Convergence for Energy & Environment (C_2E_2), School of Chemical and Biological Engineering, Seoul National University, 599 Gwanangno, Gwanakgu, Seoul 151-742, Korea

Supporting Information

ABSTRACT: Highly dispersible graphene oxide (GO) sheets of uniform submicrometer size were successfully fabricated from pristine graphite using a simple mechanochemical process. The GO flake morphology was transformed into a spherical form, and the density was decreased slightly via the ball-milling process. Ball-milled GO can be used as an electrorheological (ER) material because of its small particle size, low conductivity, and outstanding dispersibility in silicone oil. We found that the 2-h ball-milled GO-based ER fluid had the best ER performance (shear stress of 78.5 Pa and 630% ER efficiency), which was double that of the nonmilled GO-based ER fluid. The response time to form a fibrillar structure along the applied electric field direction and the recovery time to the starting level decreased with increasing ball-milling time. Additionally, the retarded settling velocity of isolated GO sheets and the electrostatic repulsion between oxygen functional groups on the GO sheets combined to improve the antisedimentation property. The ability to control the size of graphene sheets is a great opportunity to advance graphene commercialization in a high-quality, scalable production setting.

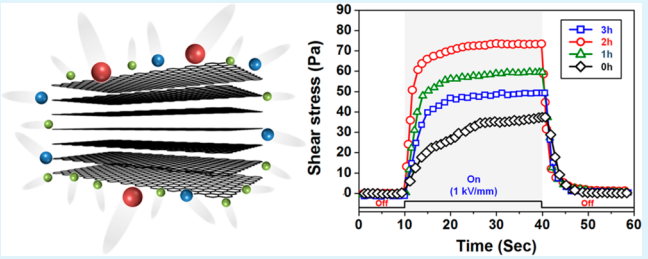

KEYWORDS: *graphene, size control, ball-milling, electrorheology, sedimentation stability*

INTRODUCTION

An electrorheological (ER) fluid is a smart and intelligent material that can change its ER properties under changing applied electric field strengths. ER fluids have attracted a great deal of interest because of several attributes, such as their simple mechanics, rapid response times, reversibility, and low power consumption.[1−4] For these reasons, ER smart materials have been widely utilized in electromechanical devices including engine mounts, ER valves, human muscle stimulators, and vibration dampers.[5−7] ER fluids are typically composed of polarizable particles dispersed in insulating oils such as silicone oils to avoid electrical short-circuiting.[8−10]

Graphene is a flat monolayer of carbon atoms tightly packed into a two-dimensional (2D) honeycomb lattice. It is regarded as a good ER material candidate because of its high surface area, unique nanostructure, and good mechanical strength.[11−14] The low electrical conductivity of graphene oxide (GO) synthesized by chemical exfoliation of graphite, without any post-treatment, makes GO of particular interest for ER applications. Furthermore, GO has hydroxyl, carboxyl, and epoxide oxygen functional groups on the basal planes and edges. These functional groups provide good dispersion stability to the GO in aqueous and organic solvents.[15−19]

Diverse synthetic strategies have been developed to fabricate GO-based ER materials. These materials include GO/TiO_2 nanocomposites, GO/polyaniline (PANI) nanocomposites, and GO-coated core−shell structured polystyrene microspheres.[20−25] However, all of these materials suffer from requiring complicated procedures and having low colloidal stabilities and a tendency to sediment, which limits their practical or industrial applications.[26] Additionally, most previous GO-based ER research has used GO having an irregular morphology and micrometer-sized particles. Despite recent advances in ER materials using GO-based nanocomposites, it is still challenging to develop easy and efficient methods to obtain GO sheets having excellent dispersibility in an insulating medium. This property is essential for the development of enhanced GO-based ER fluids.

Herein, we report a novel synthesis of highly dispersible GO sheets using a mechanochemical method. To the best of our knowledge, this is the first experimental evidence for improved dispersibility of GO sheets in silicone oil. The improved dispersibility obtained by combining ball milling and chemical exfoliation processes is derived from a narrow particle size distribution and a high degree of oxidation.[27−32] The size of the GO sheets was easily controlled by adjusting the ball-milling time. The ball-milling process transformed the morphology of the GO sheets into a spherical form. The effect of the GO size and morphology on the ER activity was investigated as a function of the shear rate, GO volume fraction, and electric field strength. The particle size distribution and sedimentation stability of synthesized GO-based ER fluids were also studied.

Received: December 23, 2013
Accepted: March 25, 2014
Published: March 26, 2014

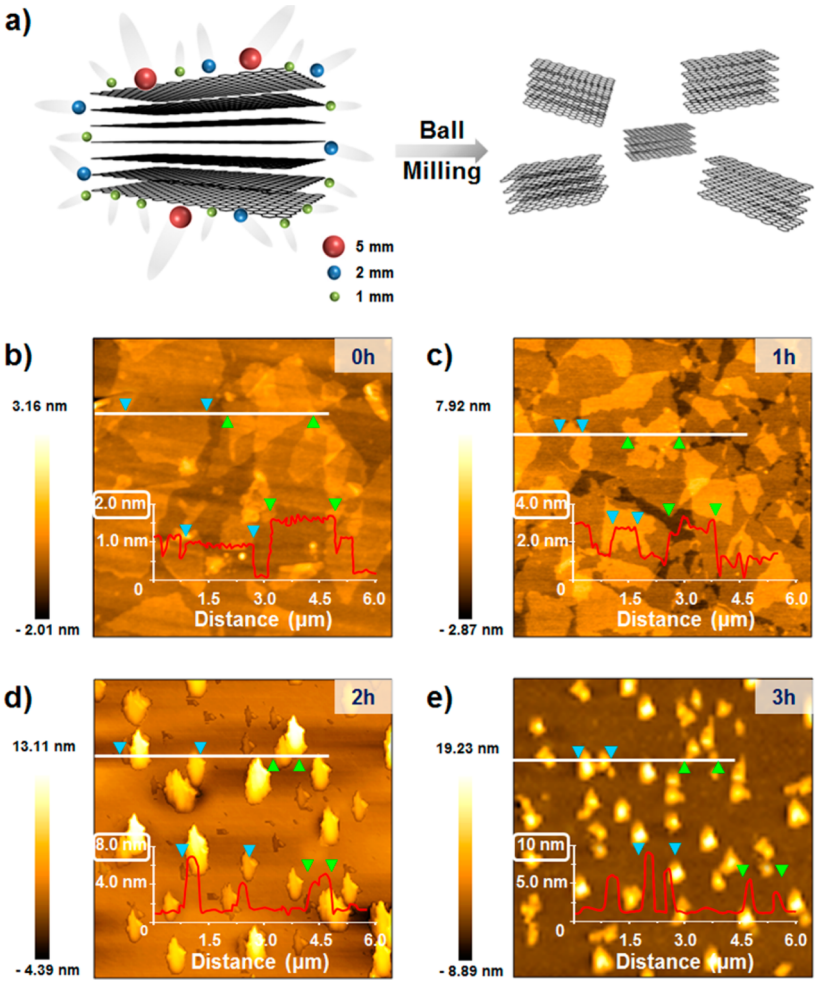

Figure 1. (a) Schematic illustration of the production of size-controlled graphite via ball milling using three balls (diameters: 1, 2, and 5 mm). (b–e) Representative AFM images of size-controlled GO as a function of ball-milling time. The GO solution was deposited on a silicon wafer for AFM analysis.

EXPERIMENTAL SECTION

Materials. Graphite (flake, <20 μm) was purchased from Sigma-Aldrich. Other reagents including $KMnO_4$, HCl, H_2SO_4, H_2O_2, and ethanol were obtained from the Aldrich Chemical Co. All regents were used as received. Distilled water was used in all of the experiments. Silicone oil (Aldrich, poly(methylphenylsiloxane), viscosity = 100 cSt) was used as a dispersing medium for electrorheological (ER) fluid applications.

Fabrication of Ball-Milled Graphite. Pristine graphite (5.0 g) was placed in a wet planetary ball-mill capsule along with three sizes of balls (diameters: 1, 2, and 5 mm). The grinding bowls and balls were made from zirconium oxide. The capsule was then fixed in the planetary ball mill and agitated at 550 rpm. The milled product was collected by sieving.

Synthesis of Size-Controlled GO Sheets. Size-controlled GO was synthesized from ball-milled graphite using a modified Hummers method. Typically, ball-milled graphite (1.0 g) was added to 70 mL of H_2SO_4 in an ice bath, followed by the addition of $KMnO_4$ (3.0 g) and $NaNO_3$ (0.5 g). After stirring for 4 h, 70 mL of distilled water was slowly added, and the suspension was kept in the ice bath for 30 min. Subsequently, H_2O_2 solution was added until the color turned a brilliant brown, which indicated complete oxidation. The ball-milled graphite oxide slurry was exfoliated to generate size-controlled GO nanosheets by sonicating for 3 h in an ultrasonic cleaner (42 kHz, 100 W, Bransonic 3510, Branson Ultrasonics Corp., Danbury, CT, USA). Finally, the mixture was separated by centrifugation, washed repeatedly with 5% HCl and distilled water, and dried in a vacuum oven at 40 °C for 24 h.

Investigation of Electrorheological Properties. All of the dried size-controlled GO samples were dispersed in silicone oil [poly(methylphenylsiloxane), viscosity = 100 cSt] for ER evaluation. No additives were added to the ER fluids. ER properties were measured with a rheometer (AR2000 Advanced Rheometer, TA Instruments) with a concentric conical cylinder geometry (cup radius: 15 mm), a temperature controller, and a high-voltage generator (Trek 677B). The gap distance was 1.00 mm. After loading a sample in the rheometer, direct current (DC) voltage was applied to the plate. The volume fraction of the ER material in the silicone oil was controlled at 0.5–3.0 vol %, and the shear rate was varied from 0.5–500 s^{-1}. All measurements were performed at room temperature. The yield stress value of prepared ER fluids is typically obtained from the flow curve of a controlled shear rate (CSR) mode experiment. The stress value of the transition point at which the shear viscosity abruptly decreased was taken as the dynamic yield stress.

Characterization. TEM images were obtained with a JEOL 6700F instrument. XPS spectra were recorded using a Kratos Model AXIS-HS system. The topography was determined by atomic force microscopy (AFM) using a Digital Instrument Nanoscope IIIA from Veeco Instruments Inc.; silicon tips were used in tapping mode at a resonance frequency of 320 kHz. Optical micrographs were taken with a Leica DM2500P microscope. The conductivity was measured for GO spin-coated from solution onto a silicon wafer (1000 rpm, 40 s). The thickness of the ball-milled GO flakes was determined by AFM analysis, and the electrical resistance was measured with a Keithley

dx.doi.org/10.1021/am405930k | ACS Appl. Mater. Interfaces 2014, 6, 5531–5537

2400 SourceMeter at 25 °C using the four-point probe method. The density of the ball-milled GO was measured using a pycnometer (25 mL). The density (ρ_p) was calculated by the equation

$$\rho_p = \frac{(W_0 - P)}{(W_2 - P) - (W_1 - W_0)} \times D$$

where P is the pycnometer mass and W_0, W_1, and W_2 are the masses of the particles, the particles and liquid, and the liquid in the bottle, respectively. The density (D) of water used as the liquid was taken as 1 g cm^{-3}.

RESULTS AND DISCUSSION

A schematic diagram of the preparation of size-controlled graphite via the ball-milling process is shown in Figure 1a. Natural flaked graphite (ca. 20 μm) is composed of layered graphene nanosheets; the carbon atoms are linked by covalent bonds. However, those carbon atoms positioned in adjacent planes are bound by much weaker van der Waals forces.[33−35] These weak interplanar forces enable the energy provided by ball-milling to provide submicrometer-sized flakes whose size can be easily controlled by the ball-milling time. Three ball sizes (diameters: 1, 2, and 5 mm) were used (Supporting Information Figure S1). Under our experimental conditions, size-controlled GO sheets were obtained from ball-milled graphite by a chemical exfoliation process according to a modified Hummers method.[36−38] Figure 1b−e shows AFM images of size-controlled GO flakes as a function of the ball-milling time. The GO sheet before ball-milling consisted of a few micrometer-sized monolayers (<1.5 nm), bilayers (2−3 nm), and multilayers (>3 nm). Ball-milling reduced the GO particles to submicrometer sizes and concurrently transformed the particle morphology from flake to spherical, with a slight increase in thickness. The transmission electron microscopy (TEM) images shown in Supporting Information Figure S2 reveal that an aqueous dispersion of ball-milled GO had a narrower particle size distribution (ca. 400−700 nm) than nonmilled GO flakes (ca. 0.6−5 μm).

X-ray photoelectron spectroscopy (XPS) was used to further understand the effect of ball-milling (Figure 2). The GO C 1s signal has three components, which correspond to the C═C/C−C in aromatic rings (284.5 eV), C−O (286.6 eV), and C═O (288.5 eV) functional groups.[39] The C−O component comes from the epoxy and hydroxyl groups, and the C═O peak originates from the carboxyl and carbonyl groups. The I_{C-O}/I_{C-C} ratio increased from 0.45 to 1.31 after 3 h of ball-milling. This increase was attributed to an increase in the surface area with decreasing GO size. Oxygen functional groups were introduced into the graphene basal and edge planes via the chemical exfoliation process. Active sites on the ball-milled GO surface could bind more oxygen functional groups because of the greatly increased surface area. The electrical conductivities of the synthesized ball-milled GO sheets were measured using a four-probe method. All of the conductivities were less than 1.0×10^{-6} S cm^{-1}, which is sufficient for a direct ER application, without requiring any post-treatment. The smaller size and high numbers of oxygen functional groups on the ball-milled graphene sheets resulted in enhanced dispersibility in silicone oil, eliminating the need for a solvent exchange process.

Figure 3a shows the shear stress and shear viscosity flow curves as a function of the shear rate for synthesized GO-based ER fluids at a volume fraction of 3 vol % under 1 kV mm^{-1} of electric field strength. Under an applied electric field, all of the

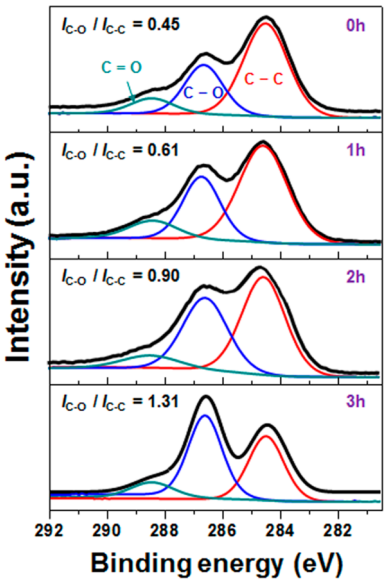

Figure 2. Deconvoluted XPS spectra in the C 1s region of size-controlled GO as a function of ball-milling time. Powdered samples were used for the XPS analysis. The fitted peaks correspond to the C−C, C−O, and C═O functional groups.

prepared ER fluids displayed a shear stress plateau region over a broad range of shear rates, typical of Bingham plastic behavior.[40,41] These results indicate that the interface of the synthesized GO began to polarize; electrostatic interactions between the GO sheets could occur through such interfacial polarization. The hydrostatic force generated by the shear flow opposed these interactions. Beyond the critical shear rate ($\dot{r}_{crit}$), the shear stress increased gradually with increasing shear rate, corresponding to typical Newtonian fluid behavior.[42,43] Notably, all of the ball-milled GO-based ER fluids displayed similar flow curves in the high shear rate region, behavior that was ascribed to shear deformation. The chainlike structure of the ER fluids began to degrade under the high shear forces in the high shear rate region; whereas, the structural stability was maintained at low shear rates. The GO-based ER fluids containing GO ball-milled for 2 h had the best ER performance. This result was attributed to the size and morphology of the graphene sheets. In terms of the graphene-based ER fluid behavior, a flake-like morphology enhances performance relative to a spherical form because of the higher shear stress applied per unit sheet area. Smaller particles can also improve the performance because of stronger dipole polarization in the chainlike structure. The permittivity (ε') was obtained as a function of the GO size (Supporting Information Figure S3). The permittivity was always greater at lower frequencies than at higher frequencies, and the addition of GO significantly improved the permittivity of the pristine silicone oil-based ER fluid. The values slightly increased with decreasing GO particle size. Ball-milling reduced the particle size and concurrently increased the number of polar groups. This facilitated the transportation of charges via rearrangement and thereby improved the permittivity of the ball-milled GO-based ER fluids. The ER characteristics reached a maximum at 2 h of ball-milling time (shear stress of 78.5 Pa at a shear rate of 1 s^{-1}); this ER efficiency was double that of the nonmilled GO-based ER fluid. The shear viscosities of the synthesized GO-based ER fluids were also measured. Apparent shear thinning behavior was clearly observed in the low shear rate region according to

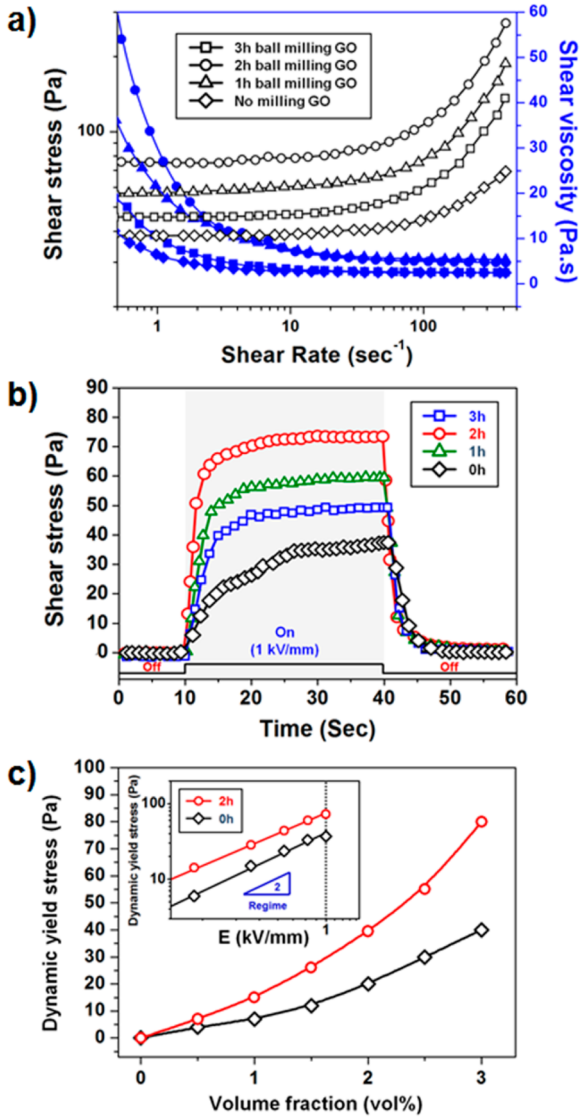

Figure 3. (a) Shear stress (open symbols) and shear viscosity (closed symbols) of size-controlled GO-based ER fluids (3 vol % in silicone oil under a 1 kV mm^{-1} electric field). (b) Effect of switching the applied electric field on the shear stress of sized-controlled GO-based ER fluids (at a shear rate of 1 s^{-1}). (c) Dynamic yield stress as a function of the volume fraction for 0- and 2-h ball-milled GO-based ER fluids under a 1 kV mm^{-1} electric field (inset: dynamic yield stress vs electric field strength).

the Bingham model. Ball-milled GO sheets with outstanding dispersibility had a relatively high off-field viscosity compared with nonmilled GO sheets. The value of the 3-h ball-milled GO-based ER fluid was ca. 0.623 Pa s, which is 2.6 times that of the nonmilled GO-based ER fluid (Table 1).

An applied electric field (1 kV mm^{-1}) was alternately turned on and off to evaluate the real-time responses of the synthesized GO-based ER fluids (Figure 3b). The shear stress values of all of the prepared ER fluids immediately increased once the electric field was applied. In contrast, the values rapidly decreased back to their original levels when the electric field was turned off. This indicates that the stress response of the prepared GO-based ER fluids was reversible and reproducible. Additionally, all of the GO-based ER fluid samples displayed low current leakage. The electric density was less than 10 μA cm^{-2} at an electric field strength of 1 kV mm^{-1}. However, the synthesized GO-based ER fluids had variable response times (t_{res}) and recovery times (t_{rec}) (defined as the time required for the response or recovery to reach 90% of its final or initial value). The response and recovery times tended to decrease with increasing ball-milling time because the size of the GO sheets affected the viscous drag forces (Table 1). Smaller GO particle sizes could potentially form chainlike structures rapidly and with higher mobility. The synthesized GO-based ER fluids also displayed significantly different ER activities in terms of their ER efficiencies (defined as $(\tau_E - \tau_o)/\tau_o \times 100$, where τ_E and τ_o are the shear stresses with and without an applied electric field strength, respectively). At a shear rate of 1 s^{-1}, 2-h ball-milled GO had a much higher ER efficiency (630%) than nonmilled GO sheets (305%).

Table 1. Electrorheological Activity of Size-Controlled GO-Based Fluids

ball-milling time[a] (h)	0	1	2	3
off-field viscosity (Pa s)	0.244	0.512	0.588	0.623
response time (s)	16.4	7.6	4.9	5.5
recovery time (s)	7.1	5.0	3.8	4.4
ER efficiency (%)	305	510	630	450

[a]The size-controlled GO was dispersed at 3 vol % in silicone oil at a shear rate of 1 s^{-1}.

The influence of the GO volume fraction (vol %) on the dynamic yield stress was evaluated for an in-depth insight into the ER activity of the synthesized GO-based ER fluids. Figure 3c shows that the yield stress increased dramatically with the GO volume fraction. Notably, the yield stress of 2-h ball-milled GO-based ER fluid at 3 vol % was 5.3 times higher than that of the same ER material at 1 vol %. Improved interplanar interactions of the GO sheets caused a greater resistance to deformation in shear flow at the higher volume fraction. Additionally, the maximum yield stress of the GO-based ER fluids increased with decreasing diameter of the GO sheets. Electrostatic interactions were sufficient to counteract the hydrodynamic interaction in shear flow stemming from the high surface area of the ball-milled GO. The relationship between the yield stress (τ_y) and the electric field strength is plotted on a log–log scale in Figure 3c (inset). As with most ER fluids, the yield stresses of all of the synthesized GO-based ER fluids were directly proportional to the square of the applied electric field strength, as indicated by the slope of 2.0, in agreement with the polarization model of the ER mechanism.[44,45]

A microstructural transition of 2-h ball-milled GO-based ER fluid was observed by optical microscopy under an applied electric field (Figure 4). An ER device with a gap distance of 1.00 mm was designed to investigate the GO-based ER fluid behavior in an electric field (Supporting Information Figure S4). Once the electric field was applied, the randomly dispersed GO sheets began to form a fibrillar structure in the direction of the applied electric field. It took only a few milliseconds to form the chainlike structure. It is known that the electrostatic interactions between ER materials are enhanced by increasing the electric field strength. The aligned fibrous structure, formed by electrostatic interactions between the GO sheets, rapidly reforms its structure under a shear force and has better resistance to shear flow. Dynamic light scattering (DLS) was used to investigate the particle size distribution of 2-h ball-milled GO in silicone oil (Figure 5a). The average diameter of the 2-h ball-milled GO particles was 3.43 μm. The inset to

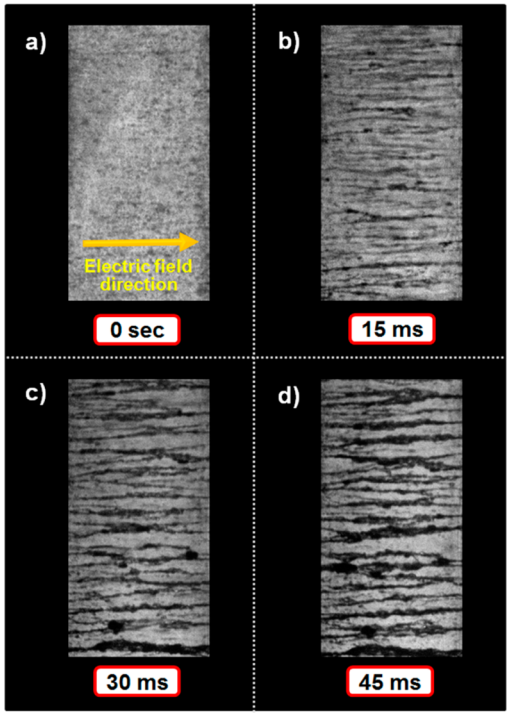

Figure 4. (a–d) Optical microscopy images of 2-h ball-milled GO dispersed at 3 vol % in silicone oil under a 1 kV mm^{-1} electric field. The gap between the two electrodes was fixed at 0.5 mm. The randomly dispersed ball-milled GO aligned with the electric field direction within a few milliseconds.

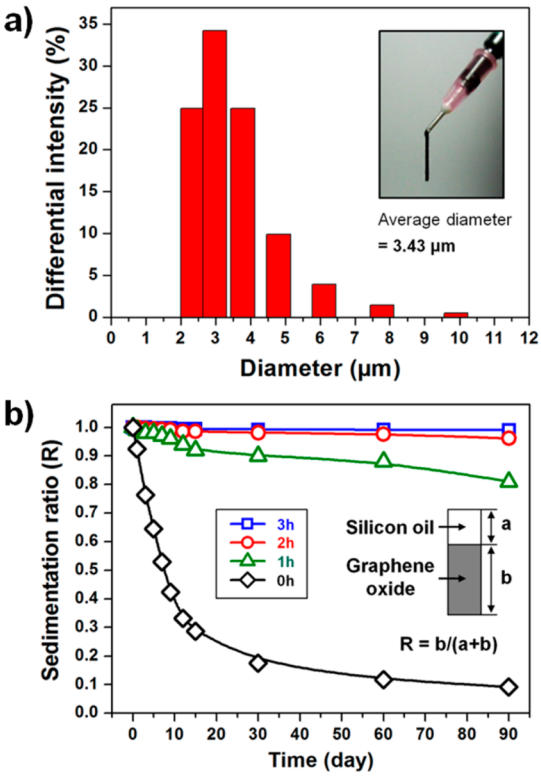

Figure 5. (a) DLS analysis of 2-h ball-milled GO dispersed at 3 vol % in silicone oil (inset: extrusion of 2-h ball-milled GO-based ER fluid from a needle). (b) Sedimentation properties of size-controlled GO-based ER fluids (3 vol % in silicone oil) (inset: definition of the sedimentation ratio).

Figure 5a shows the outstanding dispersibility in silicone oil. The 0-h ball-milled GO-based ER fluid had a broad particle size distribution, with an average diameter of 80.45 μm (Supporting Information Figure S5). These findings demonstrated that the ball-milled GO had much better dispersibility in silicone oil than 0-h ball-milled GO because of its smaller size and higher oxygen functional group content.

Notably, ball-milled GO dispersed at 3 vol % in silicone oil had a better sedimentation ratio than the equivalent nonmilled GO dispersion (Figure 5b). Increasing the ball-milling time greatly decreased sedimentation; no sediment was evident after 90 days. This superb dispersion stability relates to the sedimentation velocity, which is a significant factor in particle precipitation. Stokes' law is commonly used to calculate the rate of sedimentation; it indicates that the motion of a particle in a viscous liquid reaches an equilibrium condition having a uniform velocity or sedimentation rate. Stokes' law is expressed as follows:

$$V_g = d^2(\rho_p - \rho_l)/18\eta G$$

where V_g is the sedimentation velocity, d is the particle diameter, ρ_p is the particle density, ρ_l is the liquid density, η is the viscosity of the liquid, and G is the gravitational acceleration. Synthesized GO densities were measured using a pycnometer; the densities slightly decreased with increasing ball-milling time (Table 2). Changes in pressure or temperature can affect densities. In our experiment, ball-milled GO was obtained by chemical exfoliation of ball-milled graphite, which involved mechanical impact and heat generation. This process caused the GO flake morphology to transform into a spherical shape and increased the particle thickness and volume. This morphological transformation via the mechanochemical process played a key role in reducing the GO density. A Stokes' settling equation was used to estimate the sedimentation velocities (V_g), which were 2.590 × 10^{-8}, 2.702 × 10^{-9}, and 2.351 × 10^{-10} m s^{-1} for the 1-, 2-, and 3-h ball-milled GO, respectively (Table 2). The V_g of 2-h ball-milled GO sheets was ca. 77 times slower than that of nonmilled GO sheets. The low settling velocity of isolated GO sheets and the electrostatic repulsions between oxygen functional groups on the GO sheets are expected to have a combined effect on the antisedimentation property.

CONCLUSION

A simple and effective mechanochemical approach was used to control the size of GO sheets. GO nanosheets having outstanding dispersibility were prepared in silicone oil. The superior dispersibility was derived from the small average particle size, narrow particle size distribution, and the high degree of oxidation of the nanosheets. Ball-milling transformed the GO flake morphology into a spherical form and lowered the density slightly. The GO-based ER fluid made with GO ball-milled for 2 h had the best ER performance (shear stress of 78.5 Pa at a shear rate of 1 s^{-1}), which was double that of the nonmilled GO-based ER fluid and had fast response and recovery times under applied electric fields. The ability to control the size of a graphene sheet is an important advance toward graphene commercialization using a high-quality, scalable production process.

Table 2. Physical Parameters and Sedimentation Velocity of Size-Controlled GO in Silicone Oil

ball-milling time (h)	0	1	2	3
GO diameter[a] (nm)	600−5000	700−1500	400−700	200−300
GO thickness[a] (nm)	0.5−1.5	1.5−3	3−8	4−10
GO density[b] (g cm^{-3})	1.83	1.78	1.56	1.53
fluid density[c] (g cm^{-3})	0.97	0.97	0.97	0.97
fluid viscosity[c] (Pa s)	0.097	0.097	0.097	0.097
sedimentation velocity[d] (m s^{-1})	2.057×10^{-7}	2.590×10^{-8}	2.702×10^{-9}	2.351×10^{-10}

[a]The average GO diameter and thickness were determined by AFM and TEM analyses. [b]The GO density was measured by pycnometry at 20 °C. [c]Silicone oil (poly(methylphenylsiloxane), viscosity = 100 cSt) was used as the dispersing medium. [d]The sedimentation velocity was calculated using Stokes' equation.

■ ASSOCIATED CONTENT

Supporting Information

(1) Schematic representation of the ball-milling process, (2) TEM images of ball-milled GO, (3) permittivities of size-controlled GO-based ER fluids, (4) device designed for the study of GO-based ER fluid behavior, and (5) DLS analysis of 0-h ball-milled GO in silicone oil. This material is available free of charge via Internet at http://pubs.acs.org.

■ AUTHOR INFORMATION

Corresponding Author

*E-mail: jsjang@plaza.snu.ac.kr.

Notes

The authors declare no competing financial interest.

■ REFERENCES

(1) Hong, J.-Y.; Choi, M.; Kim, C.; Jang, J. Geometrical Study of Electrorheological Activity with Shape-Controlled Titania-Coated Silica Nanomaterials. *J. Colloid Interface Sci.* **2010**, *347*, 177−182.

(2) Yin, J.; Zhao, X.; Xiang, L.; Xia, X.; Zhang, Z. Enhanced Electrorheology of Suspensions Containing Sea-Urchin-like Hierarchical Cr-Doped Titania Particles. *Soft Matter* **2009**, *5*, 4687−4697.

(3) Cho, M.; Cho, Y.; Choi, H.; Jhon, M. Synthesis and Electrorheological Characteristics of Polyaniline-Coated Poly(methyl methacrylate) Microsphere: Size Effect. *Langmuir* **2003**, *19*, 5875−5881.

(4) Xiao, J. J.; Huang, J. P.; Yu, K. W. Dynamic Polarizability of Rotating Particles in Electrorheological Fluids. *J. Phys. Chem. B* **2008**, *112*, 6767−6771.

(5) Zhang, W. L.; Choi, H. J. Silica-Graphene Oxide Hybrid Composite Particles and Their Electroresponsive Characteristics. *Langmuir* **2012**, *28*, 7055−7062.

(6) Hong, S. R.; Choi, S. B.; Han, M. S. Vibration Control of a Frame Structure Using Electro-Rheological Fluid Mounts. *Int. J. Mech. Sci.* **2002**, *44*, 2027−2045.

(7) Niu, X.; Zhang, M.; Wu, J.; Wen, W.; Sheng, P. Generation and Manipulation of "Smart" Droplets. *Soft Matter* **2009**, *5*, 576−581.

(8) Cheng, Y.; Wu, K.; Liu, F.; Guo, J.; Liu, X.; Xu, G.; Cui, P. Facile Approach to Large-Scale Synthesis of 1D Calcium and Titanium Precipitate (CTP) with High Electrorheological Activity. *ACS Appl. Mater. Interfaces* **2010**, *2*, 621−625.

(9) Parmar, K. P. S.; Meheust, Y.; Schjelderupsen, B.; Fossum, J. O. Electrorheological Suspensions of Laponite in Oil: Rheometry Studies. *Langmuir* **2008**, *24*, 1814−1822.

(10) Sim, I. S.; Kim, J. W.; Choi, H. J.; Kim, C. A.; Jhon, M. S. Preparation and Electrorheological Characteristics of Poly(p-phenylene)-Based Suspensions. *Chem. Mater.* **2001**, *13*, 1243−1247.

(11) Hong, J.-Y.; Lee, E.; Jang, J. Electro-Responsive and Dielectric Characteristics of Graphene Sheets Decorated with TiO_2 Nanorods. *J. Mater. Chem. A* **2013**, *1*, 117−121.

(12) Yin, J.; Wang, W.; Chang, R.; Zhao, X. Polyaniline Decorated Graphene Sheet Suspension with Enhanced Electrorheology. *Soft Matter* **2012**, *8*, 294−297.

(13) Zhang, W. L.; Liu, Y. D.; Choi, H. J.; Kim, S. G. Electrorheology of Graphene Oxide. *ACS Appl. Mater. Interfaces* **2012**, *4*, 2267−2272.

(14) Zhang, W. L.; Choi, H. J. Fast and Facile Fabrication of a Graphene Oxide/Titania Nanocomposite and Its Electro-Responsive Characteristics. *Chem. Commun.* **2011**, *47*, 12286−12288.

(15) Shin, K.-Y.; Hong, J.-Y.; Jang, J. Flexible and Transparent Graphene Films as Acoustic Actuator Electrodes Using Inkjet Printing. *Chem. Commun.* **2011**, *47*, 8527−8529.

(16) Shin, K.-Y.; Hong, J.-Y.; Jang, J. Micropatterning of Graphene Sheets by Inkjet Printing and Its Wideband Dipole-Antenna Application. *Adv. Mater.* **2011**, *23*, 2113−2118.

(17) Stankovich, S.; Piner, R. D.; Chen, X. Q.; Wu, N. Q.; Nguyen, S. T.; Ruoff, R. S. Stable Aqueous Dispersions of Graphitic Nanoplatelets via the Reduction of Exfoliated Graphite Oxide in the Presence of Poly(sodium 4-styrenesulfonate). *J. Mater. Chem.* **2006**, *16*, 155−158.

(18) Stankovich, S.; Dikin, D. A.; Dommett, G. H. B.; Kohlhaas, K. M.; Zimney, E. J.; Stach, E. A.; Piner, R. D.; Nguyen, S. T.; Ruoff, R. S. Graphene-Based Composite Materials. *Nature* **2006**, *442*, 282−286.

(19) Stankovich, S.; Dikin, D. A.; Compton, O. C.; Dommett, G. H. B.; Ruoff, R. S.; Nguyen, S. T. Systematic Post-Assembly Modification of Graphene Oxide Paper with Primary Alkylamines. *Chem. Mater.* **2010**, *22*, 4153−4157.

(20) Hu, H.; Wang, X.; Wang, J.; Liu, F.; Zhang, M.; Xu, C. Microwave-Assisted Covalent Modification of Graphene Nanosheets with Chitosan and Its Electrorheological Characteristics. *Appl. Surf. Sci.* **2011**, *257*, 2637−2642.

(21) Zhang, W. L.; Liu, Y. D.; Choi, H. J. Graphene Oxide Coated Core−Shell Structured Polystyrene Microspheres and Their Electrorheological Characteristics under Applied Electric Field. *J. Mater. Chem.* **2011**, *21*, 6916−6921.

(22) Hiamtup, P.; Sirivat, A.; Jamieson, A. M. Strain-Hardening in the Oscillatory Shear Deformation of a Dedoped Polyaniline Electrorheological Fluid. *J. Mater. Sci.* **2010**, *45*, 1972−1976.

(23) Yin, J.; Chang, R.; Shui, Y.; Zhao, X. Preparation and Enhanced Electro-Responsive Characteristic of Reduced Graphene Oxide/Polypyrrole Composite Sheet Suspensions. *Soft Matter* **2013**, *9*, 7468−7478.

(24) Yin, J.; Shui, Y.; Chang, R.; Zhao, X. Graphene-Supported Carbonaceous Dielectric Sheets and Their Electrorheology. *Carbon* **2012**, *50*, 5247−5255.

(25) Yin, J.; Chang, R.; Kai, Y.; Zhao, X. Highly Stable and AC Electric Field-Activated Electrorheological Fluid Based on Mesoporous Silica-Coated Graphene Nanosheets. *Soft Matter* **2013**, *9*, 3910−3914.

(26) Hong, J.-Y.; Jang, J. Molecular Dynamics Simulation Studies of Platelets with Square Cross-Sectional Area: Formation of a Stable Cubatic Phase. *Soft Matter* **2012**, *8*, 3348−3350.

(27) Jeon, I.-Y.; Choi, H.-J.; Choi, M.; Seo, J.-M.; Jung, S.-M.; Kim, M.-J.; Zhang, S.; Zhang, L.; Xia, Z.; Dai, L.; Park, N.; Baek, J.-B. Surface Engineered Porous Silicon for Stable, High Performance Electrochemical Supercapacitors. *Sci. Rep.* **2013**, *3*, 1−7.

(28) Yue, X.; Wang, H.; Wang, S.; Zhang, F.; Zhang, R. In-Plane Defects Produced by Ball-Milling of Expanded Graphite. *J. Alloys Compd.* **2010**, *505*, 286−290.

(29) Zhao, W.; Fang, M.; Wu, F.; Wu, H.; Wang, L.; Chen, G. Preparation of Graphene by Exfoliation of Graphite Using Wet Ball Milling. *J. Mater. Chem.* **2010**, *20*, 5817−5819.
(30) Duan, W. Nanostructure Evolution of Expanded Graphite during High-Energy Ball-Milling. *Appl. Mech. Mater.* **2011**, *80*−*81*, 229−232.
(31) Welham, N. J.; Berbenni, V.; Chapman, P. G. Effect of Extended Ball Milling on Graphite. *J. Alloys Compd.* **2003**, *349*, 255−263.
(32) Chen, Y.; Qian, J.; Cao, Y.; Yang, H.; Ai, X. Green Synthesis and Stable Li-Storage Performance of $FeSi_2$/Si@C Nanocomposite for Lithium-Ion Batteries. *ACS Appl. Mater. Interfaces* **2012**, *4*, 3753−3758.
(33) Shin, K.-Y.; Hong, J.-Y.; Lee, S.; Jang, J. High Electrothermal Performance of Expanded Graphite Nanoplatelet-Based Patch Heater. *J. Mater. Chem.* **2012**, *22*, 23404−23410.
(34) Tang, Q.; Wu, J.; Li, Q.; Lin, J. High Conducting Multilayer Films from Poly(sodium styrenesulfonate) and Graphite Nanoplatelets by Layer-by-Layer Self-Assembly. *Polymer* **2008**, *49*, 5329−5548.
(35) Pan, Y. X.; Yu, Z.; Ou, Y.; Hu, G. A New Process of Fabricating Electrically Conducting Nylon 6/Graphite Nanocomposites via Intercalation Polymerization. *J. Polym. Sci., Part B: Polym. Phys.* **2000**, *38*, 1626−1633.
(36) Shin, K.-Y.; Cho, S.; Jang, J. Graphene/Polyaniline/Poly(4-styrenesulfonate) Hybrid Film with Uniform Surface Resistance and Its Flexible Dipole Tag Antenna Application. *small* **2013**, *9*, 3792−3798.
(37) Hummers, W. S.; Offeman, R. E. Preparation of Graphitic Oxide. *J. Am. Chem. Soc.* **1958**, *80*, 1339.
(38) Kovtyukhova, N. I. Layer-by-Layer Assembly of Ultrathin Composite Films from Micron-Sized Graphite Oxide Sheets and Polycations. *Chem. Mater.* **1999**, *11*, 771−778.
(39) Shin, K.-Y.; Hong, J.-Y.; Lee, S.; Jang, J. Evaluation of Anti-Scratch Properties of Graphene Oxide/Polypropylene Nanocomposites. *J. Mater. Chem.* **2012**, *22*, 7871−7879.
(40) Seo, Y. P.; Seo, Y. Modeling and Analysis of Electrorheological Suspensions in Shear Flow. *Langmuir* **2012**, *28*, 3077−3084.
(41) McIntyre, C.; Yang, H.; Green, P. F. Electrorheology of Suspensions Containing Interfacially Active Constituents. *ACS Appl. Mater. Interfaces* **2013**, *5*, 8925−8931.
(42) Yin, J. B.; Zhao, X. P. Preparation and Electrorheological Activity of Mesoporous Rare-Earth-Doped TiO_2. *Chem. Mater.* **2002**, *14*, 4633−4640.
(43) Kim, J. C.; Seo, M.; Hillmyer, M. A.; Francis, L. F. Magnetic Microrheology of Block Copolymer Solutions. *ACS Appl. Mater. Interfaces* **2013**, *5*, 11877−11883.
(44) Tao, R.; Jiang, Q. Simulation of Structure Formation in an Electrorheological Fluid. *Phys. Rev. Lett.* **1994**, *73*, 205−208.
(45) Stenicka, M.; Pavlinek, V.; Saha, P.; Blinova, N. V.; Stejskal, J.; Quadrat, O. The Electrorheological Efficiency of Polyaniline Particles with Various Conductivities Suspended in Silicone Oil. *Colloid Polym. Sci.* **2009**, *287*, 403−412.